

# Simulation of Electron Beam Dynamics in a Nonmagnetized High-Current Vacuum Diode

S.Anishchenko and A.Gurinovich

Research Institute for Nuclear Problems, Belarusian State University, Minsk, Belarus

Ryazan State RadioEngineering University, 59/1 Gagarina Street, Ryazan 390005, Russia

Email: gur@inp.bsu.by

**Abstract**—The electron beam dynamics in a nonmagnetized high-current vacuum diode is analyzed for different cathode-anode gap geometries. The conditions enabling to achieve the minimal initial momentum spread in the electron beam are found out. A drastic rise of current density in a vacuum diode with a ring-type cathode is described. The effect is shown to be caused by electrostatic repulsion.

**Index Terms**—high-current electron beam, momentum spread, nonmagnetized vacuum diode

## I. INTRODUCTION

The idea to simulate the electron beam dynamics in the cathode-anode gap stems from the need to elucidate some of the results obtained in the experimental study of an axial resonant cavity vircator [1], [2] and to achieve a better understanding of the simulation results for various vircator configurations [3]–[5].

First, it was discovered that radiated power revealed a very strong dependence on the cathode geometry: the maximum radiated power was observed in the experiments with a cathode, for which emission was confined to an annular ring on a flat cathode surface (ring-type cathode) with a certain inner-to-outer diameter ratio [1], [2]. Experiments with the cathode of the same shape and size, but with solid emission surface (solid cathode) carried out in similar conditions gave the twice smaller radiated power. Similar results were obtained by the authors of [6]–[10] who reported the sensitivity of radiated power to cathode material, shape, and cathode-anode gap.

Unfortunately, despite the apparently identical experimental conditions we failed to obtain a stable maximum-power level signal.

In addition, in the experiments with a ring-type cathode, an extremely fast (after 3–4 shots) anode mesh damage in the center was observed, whereas for solid cathodes such effect was absent.

The most recent experimental and theoretical research of ring-type cathodes revealed the effect of high-current electron beam cumulation [11].

Another factor that motivated the study of the beam behavior in the cathode-anode gap was necessity to specify electron beam parameters for XOPIC simulation of axial vircator behavior (XOPIC simulates the electron beam behavior just behind the anode mesh).

Thus, to set the initial parameters of the beam for further simulation, one should know the parameters of the beam leav-

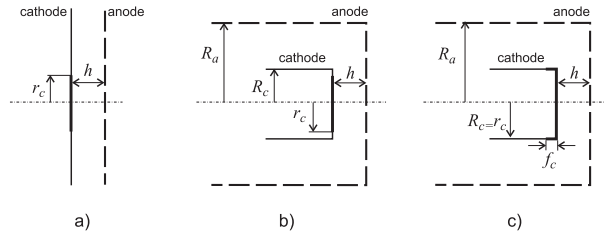


Fig. 1. Cathode-anode gap geometries

ing the cathode-anode gap. For this reason, such parameters should be either determined experimentally or calculated by simulating the electron beam dynamics in the cathode-anode gap. Finally, the initial (unrelated to the oscillations of the electrons reflected from the virtual cathode) momentum spread of the electron beam was a subject of study. (According to several publications [3], [12], [13] this type of momentum spread could also affect the operation efficiency of the vircator.) From this standpoint the electron beam dynamics in a vacuum diode is discussed in present paper. Explosive emission is simulated with a slightly modified hybrid code [17], [18], computing the electron and plasma motion in different approximations: beam dynamics – in kinetic and inhomogeneous plasma expansion - in hydrodynamic, thus decreasing the runtime noticeably. Particularly, the paper analyzes the electron beam parameters, depending on the cathode-anode gap geometry. The conditions providing the minimal momentum spread in the electron beam are obtained along with the distributions of current density over the beam radius.

A 2D simulation (the system is assumed to be axially symmetric) is carried out for three cases (Fig.1):

- infinite plane anode and infinite cathode with emitting surface of radius  $r_c$
- fixed-size plane anode (of radius  $R_a$ ) and variable size plane cathode (of radius  $R_c$ ) with emitting surface of radius  $r_c$
- fixed-size plane anode and variable size shaped cathode

## II. MOMENTUM SPREAD

Motion of electrons in a cathode-anode gap of nonmagnetized vacuum diode is determined by accelerating field applied to the gap, electrostatic repulsion and electron beam com-

pression by self-induced magnetic field. Contributions from the last two factors depend on gap geometry. Simultaneously they both also determine initial momentum spread in the diode. At the conducting surface of the cathode and anode electric field has zero tangential component. When the cathode (anode) size significantly exceeds the gap value the electron beam compression mainly contributes to the radial motion (and beam momentum spread) of beam electrons while the space-charge repulsion is low. Electrons emitted near the cathode edge get into the locally nonuniform accelerating field and undergo stronger repulsion than those by an axis. When the cathode (anode) size is close to or smaller than the gap value the repulsion effect on the radial velocity (and beam momentum spread) emerges in the foreground. As the two factors give opposite response on momentum spread when the cathode (anode) size is changed, the diode geometry enabling to achieve the minimal initial momentum spread in the electron beam is expected to exist. The following analysis is made to find out these conditions.

The analysis is made at fixed values of cathode-anode distance  $h$ ; only the radius  $r_c$  of the emitting surface is varied. In cases b and c in Fig.1, the anode radius  $R_a$  is kept fixed for these simulations and exceeds the value of  $h$  ten times. To aid in comparison of different geometries, all the results are presented in terms of  $r_c/h$  ratio.

The momentum spread

$$\Delta p_z/p_z = \frac{\sqrt{\left| \frac{1}{N_\alpha} \sum_\alpha p_{z\alpha}^2 - \left( \frac{1}{N_\alpha} \sum_\alpha p_{z\alpha} \right)^2 \right|}}{\frac{1}{N_\alpha} \sum_\alpha p_{z\alpha}} \quad (1)$$

is analyzed at a distance  $h/15 = 0.1$  cm before the anode mesh and at constant voltage values applied to the cathode: 256 kV and 511 kV. The results are compared for 3 cases: (a) infinite plane anode and infinite cathode with emitting surface of radius  $r_c$  (Fig.1a); (b1) fixed-size plane anode and plane cathode of radius  $R_c$  equal to fixed-size radius of the emitting surface,  $r_c$  (Fig.1b); (b2) fixed-size plane anode and plane cathode whose radius  $R_c > r_c$  (Fig.1b).

In the presence of an electric field in the cathode anode gap, the increase in  $r_c/h$  results in growth of the emitting current and the momentum spread (Fig.2). The momentum spread is larger the higher cathode voltage is (the same result is obtained in [15]).

The influence of field distortion at the cathode edges is evident when collating Fig.2 with Fig.3, showing the momentum spread  $\Delta p_z/p_z$  as a function of  $r_c/h$ .

For a plane cathode of radius  $R_c = r_c$ , at  $R_c < 2h$  the momentum spread grows with  $R_c/h$  decreasing. The  $R_c/h$  value corresponding to the momentum spread minimum depends on the applied voltage.

The analysis of case (b2) gives a recipe for reducing the momentum spread at small  $r_c/h$  ratios for a finite-size cathode: an increase in the cathode brim (the difference  $(R_c - r_c)$ ) enables the transition from case (b1) to case (a). In the

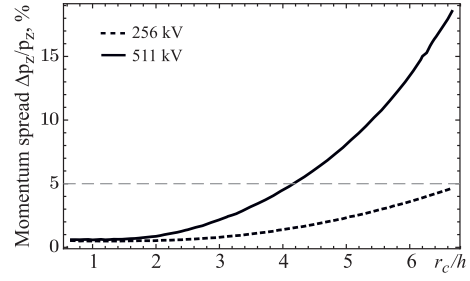


Fig. 2. Momentum spread  $\Delta p_z/p_z$  for case (a) at  $h = 1.5$  cm

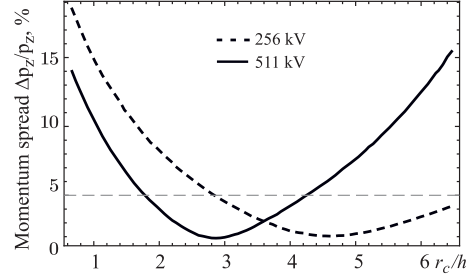


Fig. 3. Momentum spread  $\Delta p_z/p_z$  for case (b1) at  $h = 1.5$  cm and  $R_a = 15$  cm

considered example (Fig.4), the momentum spread for a finite-size cathode at  $h = 1.5$  cm,  $R_a = 15$  cm, and  $R_c - r_c \sim 1$  cm coincides with that for infinite-size cathode.

Being rather conceptual, the above investigation, however, gives explicit guidelines on how to match the sizes of the cathode (cathode brim), the emitting area and the cathode-anode gap so as to provide the lowermost momentum spread in the produced electron beam.

When describing a real experiment, one should consider the shape of voltage pulse, plasma expansion and emission from the cathode edges (see Fig.1c). For further simulation, the voltage pulse (2) with a maximal value of 400 kV is used

$$U(t) = 4 \cdot 10^5 \frac{(1 + \alpha) \alpha^{-1 + \frac{1}{1+\alpha}}}{e^{-\alpha \frac{t}{t_p}} + e^{\frac{t}{t_p}}}, \quad (2)$$

where  $t_p = 330$  ns and  $\alpha = 10$ . The plasma expansion speed is supposed to be 2 cm/ $\mu$ s, the electric field strength sufficient for explosive emission start is 150 kV/cm,  $R_a = 15$  cm, and  $h = 1.5$  cm. Solid and ring-type cathodes are considered to

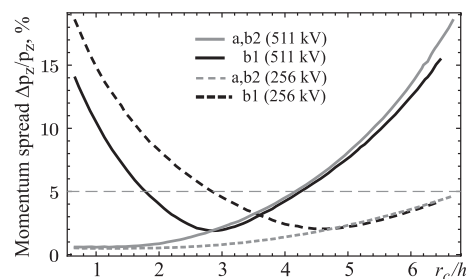


Fig. 4. Comparison of momentum spread for cases (a), (b1), and (b2) at  $h = 1.5$  cm,  $R_a = 15$  cm, and  $R_c - r_c = 1$  cm.

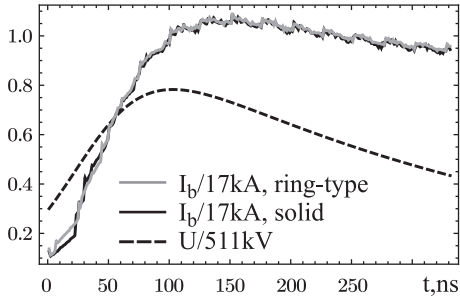


Fig. 5. Normalized beam current for the ring-type and solid cathodes and voltage pulse (2) normalized to 511 kV

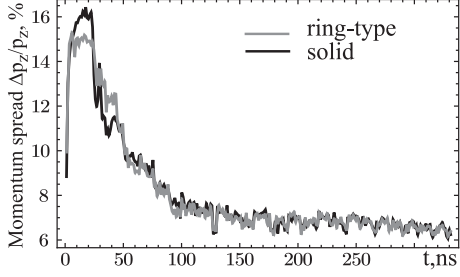


Fig. 6. Momentum spread  $\Delta p_z/p_z$  for solid and ring-type cathodes

have the outer radii  $r_c = R_c = 3$  cm; the inner cathode radius for the ring-type cathode is  $r_{c1} = 1.3$  cm. The beam current normalized to  $mc^3/e = 17$  kA for the ring-type and solid cathodes and the voltage pulse (2) normalized to 511 kV are shown in Fig. 5.

For both cathode types the produced beam current (beam impedance) is solely determined by the outer radius of the emitting surface. While the momentum spread  $\Delta p_z/p_z$  for the ring-type cathode initially appears to be a little bit lower as compared to that for the solid one, but in a short time ( $< 50$  ns) the difference diminishes (see Fig. 6). It should also be mentioned that for the considered geometry (Fig. 1c), the momentum spread is rather high. Perhaps, the cathode brim could reduce the momentum spread.

Let us consider the typical behavior of the electric and magnetic fields illustrated by a diode with the cathode-anode gap  $h = 1.5$  cm and a solid cathode of 3 cm radius. As is seen in Figs. 8 and 9, the radial component  $E_r$  of the electric field and the magnetic field  $B_\varphi$  increase as the distance  $r$  from the diode axis is increased until  $r$  becomes equal to the cathode radius, after which the fields start decreasing. Let us note that substantially different from zero values of the electric-field radial component responsible for the radial repulsion force are concentrated near the periphery of the cathode. The force  $eE_r$  acting on the relativistic particles decreases appreciably as the particles come closer to the anode. This happens due to vanishing the tangential component of the electric field at the conducting surface (anode).

The minimum in the momentum spread arises from the combined effects of two competing processes: Coulomb repulsion between charged particles and pinching of the electron

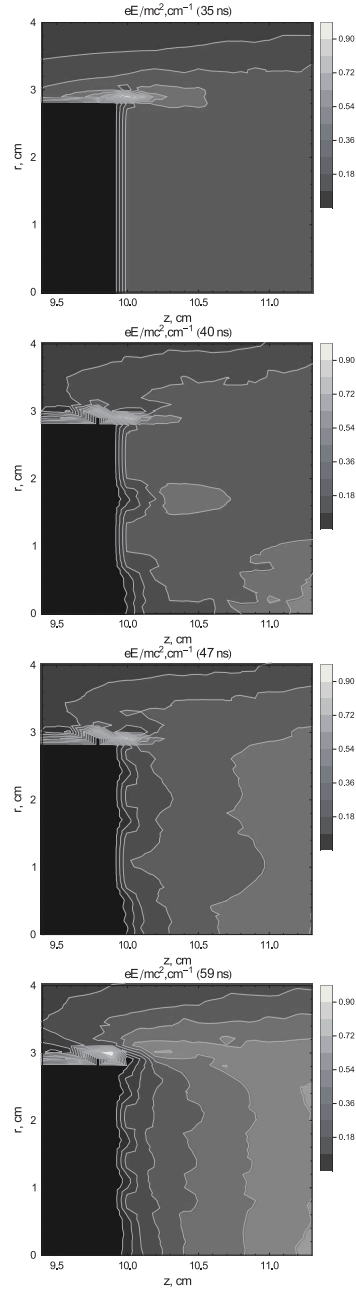


Fig. 7. Electric field strength near the surface of the solid cathode at 35ns, 40ns, 47ns and 59ns

beam by the self-induced magnetic field. At small cathode radius, the radial Coulomb repulsion prevails, being most intense near the external edge of the cathode, whereas at large radius, the compression by the self-induced magnetic field starts to dominate. Both processes lead imparting a radial momentum to the beam electrons. At a certain value of the radius, the Coulomb repulsion reduces the effect produced by the self-induced magnetic field, and pinching does not occur. The electrons arriving at the anode have the same energies; the increase in the radial velocity is accompanied by the decrease in the longitudinal one. Because different increments

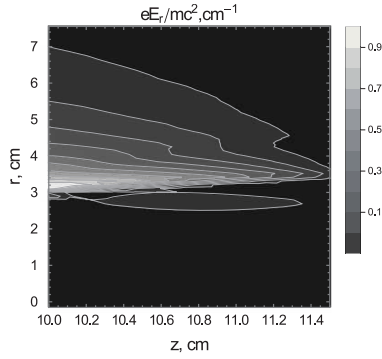


Fig. 8. Radial electric field

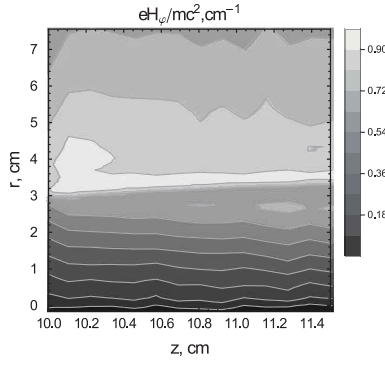


Fig. 9. Magnetic field

are imparted to the momenta of the electrons escaping from the cathode at different distances from the system axis, the observed momentum spread occurs.

For an infinite plane cathode with finite emitting surface (Fig.1a), the effects of Coulomb repulsion slacken (Fig.2) because the radial component of the electric field vanishes identically along the entire conducting surface of the cathode. No additional sharpening occurs in the electric field repulsing the particles. As a result, radial motion of the beam is determined by the magnetic field increasing as the radius of the emitting surface is increased.

### III. CURRENT DENSITY DISTRIBUTION

The developed code also enables getting the time picture of beam generation and evaluating the contribution coming from different cathode regions to the produced current. The emission from both solid and ring-type cathodes starts mainly from the cathode outer edge, and no difference between the two cathode types is observed during the first  $5 \div 10$  ns. After a short time ( $< 50$  ns), the whole surface of the solid cathode emits almost uniformly with some local current density spikes approximately twice as high as the average current density value. The distance between these spikes correlates with the distance between the cathode jets (these spikes are manifestation of nonuniformity of expanding plasma surface discussed in previous subsection). For the ring-type cathode, the current distribution near the cathode center grows rapidly after the

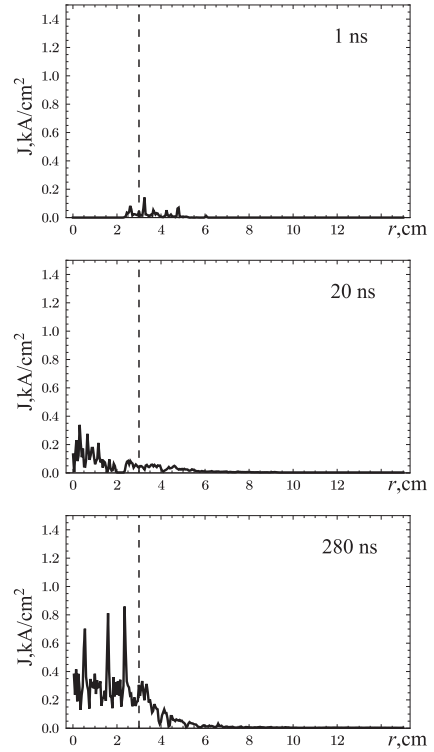


Fig. 10. Current density evolution for the solid cathode, dashed vertical line marks the cathode radius  $r_c$

first 10 ns and remains several times higher than the average current density value.

For both cathodes the beam diameter exceeds the cathode diameter approximately 1.5 times.

The explosive electron emission is most intense from the nonplanar regions of the cathode, particularly, from its inner edge. Due to Coulomb repulsion, charged particles make their way to the region that is not occupied by the beam. As a consequence, at the axis of a relativistic vacuum diode, the density of a high-current beam significantly exceeds the average current density in the cathode-anode gap.

A similar mechanism leads to the formation of current-density peaks (maxima) (Figs.10,11). The electrons that escape from the convex explosive-emission center are repulsed. The interaction between these repulsing microflows gives rise to peaks and dips in the current density distribution (Figs.10,11).

As the distance between emission centers on the cathode surface is determined by risetime of voltage pulse applied to the cathode, plasma expansion speed and some other factors. For the parameters used for simulation (voltage pulse risetime 30ns, plasma expansion speed 2 cm/mus) this distance is about 0.5-1cm. The same distance the peaks in Figs.10,11 are spaced. Typical space mesh step and time-step are as small as 0.05 cm and 1.3 ns, respectively. Therefore, the peaks are perfectly resolved.

### IV. CONCLUSION

The electron beam dynamics in a vacuum diode has been simulated. The guidelines on how to match the size of the

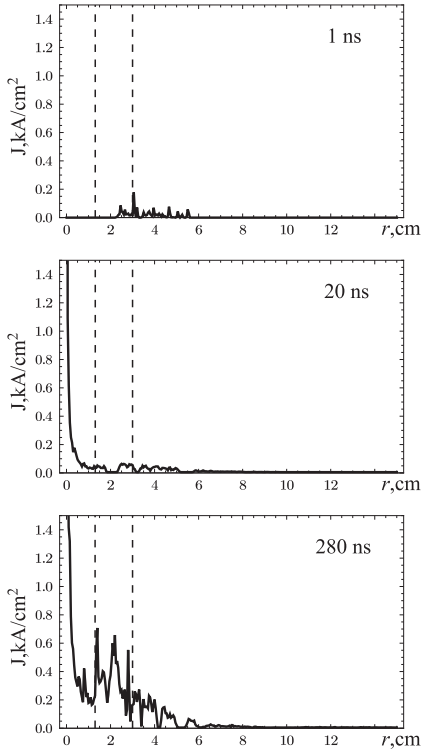


Fig. 11. Current density evolution for the ring-type cathode, dashed vertical lines mark the cathode outer  $r_c$  and inner  $r_{c1}$  radii

cathode (cathode brim), the emitting area, and the cathode-anode gap for getting the lowermost momentum spread in the produced electron beam have been developed. The distributions of current density over the beam radius obtained for both solid and ring-type cathodes enable explaining the anode mesh burning in the center in the case of a ring-type cathode.

#### ACKNOWLEDGMENT

The authors would like to thank Prof. Vladimir Baryshevsky for incentive and valuable discussions.

This research was funded by Ministry of Education and Science of Russian Federation, grant no. 14.577.21.0092 project ID RFMEFI57714X0092.

#### REFERENCES

- [1] V. Baryshevsky, A. Gurinovich, E. Gurnevich and P. Molchanov, Experimental Study of an Axial Vircator with Resonant Cavity, Proceedings of EAPPC2014, OA1.5
- [2] V. Baryshevsky, A. Gurinovich, E. Gurnevich and P. Molchanov, Experimental Study of an Axial Vircator with Resonant Cavity, IEEE Trans. Plasma Sci. (2015) doi:10.1109/TPS.2015.2439332

- [3] E. Gurnevich, P. Molchanov, The Effect of the Electron-Beam Parameter Spread on Microwave Generation in a Three-Cavity Axial Vircator, IEEE Transactions on Plasma Sci. vol.43, no.4, pp.1014 – 1017, doi: 10.1109/TPS.2015.2407492.
- [4] P.V. Molchanov, E.A. Gurnevich, V.V. Tikhomirov, S.E. Siahlo, Simulation of an axial vircator with a three-cavity resonator, arXiv:1408.1824
- [5] V.V. Tikhomirov, S.E. Siahlo, Simulation of an Axial Vircator, arXiv:1309.6486
- [6] V.L. Granatstein and I. Alexeff, *High Power Microwave Sources*. Boston, MA: Artech House, 1987, ch. 13. (p. 490), ch.14 (p.539).
- [7] Ki Baek Song, Jeong Eun Lim, Yoonho Seo, and Eun Ha Choi, Output Characteristics of the Axially Extracted Virtual Cathode Oscillator With a Cathode-Wing, IEEE Trans. Plasma Sci., v.37, no.2, (2009) 304
- [8] M. Karlsson, F. Olsson, S-E. Wippa, J. Axinger, B.O. Bergman, Experimental studies of an axial vircator with different cathode geometries, Proc. 16th IEEE International Pulsed Power Conference (2007) 780, DOI:10.1109/PPPS.2007.4651956
- [9] Anatoli S. Shlapakovski, Tal Kweller, Yoav Hadas, Yakov E. Krasik, Sergey D. Polevin, and Ivan K. Kurkan, Effects of Different Cathode Materials on Submicrosecond Double-Gap Vircator Operation, IEEE Trans. Plasma Sci., v.37, no.7 (2009) 1233.
- [10] Mattias Elfsberg, Tomas Hurtig, Anders Larsson, Cecilia Müller, and Sten E. Nyholm, Experimental Studies of Anode and Cathode Materials in a Repetitive Driven Axial Vircator, IEEE Trans. Plasma Sci., v.36, no. 3 (2008) 688.
- [11] S.V. Anishchenko, V.G. Baryshevsky, N.A. Belous, A.A. Gurinovich, E.A. Gurinovich, E.A. Gurnevich, P.V. Molchanov, Cumulation of High-current Electron Beams: Theory and Experiment, LANL e-print arXiv:1509.00522 [physics.acc-ph]
- [12] W. B. Bridges and C. K. Birdsall, Space-charge instabilities in electron diodes. J. Appl. Phys., vol. 34, no. 10, 1963, P. 2946-2955.
- [13] D. J. Sullivan, High Power Microwave Generation From a Virtual Cathode Oscillator (Vircator), IEEE Trans. on Nuc. Sci., vol. NS-30, no 4, 1983, P. 3426 - 3428.
- [14] S.P. Bugaev, E.A. Litvinov, G.A. Mesyats, and Proskurovskii, Explosive emission of electrons, Sov. Phys.-Usp., Vol. 18. No. 1, 1975, P. 51–61.
- [15] S.P. Bugaev, et al, in *Relativistic High Frequency Electronics*, Gorky, 1979, p.5.
- [16] Mesyats G A 2005 *Pulsed Power* (New York: Springer)
- [17] S. Anishchenko, A. Gurinovich, Modeling of high-current devices with explosive electron emission, Journal of Physics: Conference Series 490 (2014) 012116.
- [18] S.V. Anishchenko and A.A. Gurinovich, Modeling of high-current devices with explosive electron emission, Comput. Sci. Disc. 7 (2014) 015007
- [19] F.H. Harlow, The Particle-In-Cell Computing Method for Fluid Dynamics, Methods Comput. Phys. 1964. Vol. 3. P. 319.
- [20] F. Brunel, J.N. Leboeuf, T. Tajima, J.M. Dawson, and M. Makino, Magnetohydrodynamic Particle Code: Lax - Wendroff A Igorithm with Finer Grid Interpolations, J. Comput. Phys. 43. 268 (1981).
- [21] D.W. Hewitt and A.B. Langdon, Electromagnetic direct implicit plasma simulation, J. Comput. Phys. 1987. Vol. 72. 121.
- [22] A.G. Sveshnikov and S.A. Jakunin. Matematicheskoe Modelirovanie. 1989. Vol. 1. No. 4. P. 1-25 [in Russian].
- [23] J.P. Verboncoeur, Particle Simulation of Plasmas: Review and Advances, Plasma Phys. Control. Fusion. 2005. Vol. 47. P. 231.
- [24] J. W. Poukey, J. R. Freeman, G. Yonas, Simulation of relativistic electron beam diodes, J. Vac. Sci. Technol. 1973. Vol. 10. No. 6. P. 954.
- [25] G.T. Golovin, Numerical solution of the self-consistent problem of the transport of several electron beams, USSR Comp. Math. and Math. Phys., Vol. 23, no.2, 1983, P. 8791.
- [26] D. R. Welch, D. V. Rose, N. Bruner, R. E. Clark, B. V. Oliver, K. D. Hahn, and M. D. Johnston, Hybrid simulation of electrode plasmas in high-power diodes, Phys. Plasmas. 2009. Vol. 16. P. 123102.